Characterizing Indoor Wireless Channels via Ray Tracing Combined with Stochastic Modeling

Aliye Özge Kaya, *Student Member, IEEE,* Larry J. Greenstein, *Life Fellow, IEEE,* and Wade Trappe, *Member, IEEE*

***Abstract*—We investigate the reliability of radio channel simulators in predicting channel responses throughout a well-specified environment. Indoor environments for which the geometric layout and material properties of surfaces are known lend themselves to such site-specific simulation. We assess the performance of this approach by comparing its predictions with measurements in a specific static environment. The good agreement on path loss, Ricean K-factor and RMS delay spread, over the set of paths measured and simulated, suggests that a well-designed radio simulator can be used reliably to predict system behavior.**

Typically, wireless channel models obtained through this or similar techniques do not capture the temporal variability in the channel response due to people movement in the environment. We treat the time-varying part of the channel response using stochastic processes. Using channel sounding experiments for several typical office scenarios, we show that autoregressive processes can be used to model the time-varying tap gains for several different motion scenarios.

***Index Terms*—Indoor wireless channels, radio channel simulators, ray tracing, RMS-delay spread, K-factor, path gain, autoregressive processes, ARIMA.**

I. Introduction

In wireless communications, the underlying radio channel properties strongly affect the performance of the system. It is common practice in the design and evaluation studies of such systems to use mathematical models for describing the channel. One approach is stochastic modeling, in which the key properties of the signal propagation (e.g., multipath fading) are captured by probability distributions. These kinds of models are favored when the propagation environment is unknown except for some high-level attributes, e.g., urban vs. suburban, flat vs. hilly, summer vs. winter, etc.

Stochastic models serve well when the study questions are fairly generic, e.g., how does a particular cellular radio system perform in an environment that is typically urban? However, there are cases where the interest pertains to a specific environment, e.g., a wireless LAN in the corporate offices of a specific company. In such cases, the study questions are 'site-specific' and so site-specific channel response information is needed. One very effective approach in that case might be to measure channel responses for a very large population of transmit-receive (T-R) paths and store them in a database that can be accessed for system simulations. The number of such paths that must be sampled, however, can be extremely large and require measurement campaigns that are long, labor-intensive and costly.

An alternative that is less precise in terms of channel description but also far less costly is to use *environment simulators*. These are computer programs that (1) emulate the physical environment; and (2) use wave propagation physics to predict the radio signal produced at any receive point from any transmit point. When the physical layout is well-specified, such as indoor areas where the layouts and materials of walls, floors and ceilings are known, environment simulation can be employed on a very large scale with very little effort. The question is whether such simulation tools reliably capture the radio channel behaviors in the specified environment.

Ray tracing-based methods are popular for predicting the site-specific radio propagation characteristics [1], [2], [3], [4]. Although they are computationally intensive, they provide more accurate results than statistical models [1] when the site geometries are known.

It is axiomatic that no typical environment can be perfectly emulated. Propagating radio signals are affected by countless artifacts that are hard to capture and/or predict, i.e., moldings, variations in material, furniture, etc. What can reasonably be expected, however, is that a site-specific program predicts channel responses throughout the area of interest that are statistically similar to the actual ones. To this end, we can cite three parameters of a radio path that largely typify its response for both narrow and wide bandwidths. They are: (1) the *path loss*, *PL*, which is the dB value of the transmit power divided by the (locally averaged) received power; (2) the *Ricean K-factor*, which, together with *PL*, dictates the narrowband fading distribution; and (3) the *RMS delay spread*, τ_{rms}, which is a measure of the frequency selectivity (or pulse dispersion) of the channel. We assert that a site-specific program that accurately predicts these three quantities throughout a known environment can be relied upon to predict performance in that environment.

In this paper, we consider a particular environment, namely, the ORBIT Laboratory of Rutgers University's WINLAB [5], [6]; and we test a particular simulator, namely, the Wireless Systems Engineering (WiSE) Tool, a ray-tracing program developed by Bell Labs [7]. For a total of 18 chosen transmit-receive (T-R) paths, we use a Vector Network Analyzer

Manuscript received June 13, 2008; revised November 12, 2008 and February 11, 2009; accepted May 6, 2009. The associate editor coordinating the review of this paper and approving it for publication was G. Durgin.

Portions of this paper were presented at MILCOM 2008 and at GLOBECOM 2008. This work was supported via NSF grants CNS-0626439, CNS-0716400, and DARPA contract W31P4Q-07-1-0002.

The authors are with WINLAB, Rutgers University, NJ (e-mail: {ozgekaya, ljg, trappe}@winlab.rutgers.edu).

Digital Object Identifier 10.1109/TWC.2009.080785

(VNA) to measure complex frequency responses over a wide bandwidth, i.e., from 3 to 4 GHz; and we use WiSE to predict the impulse response. From both, we can compute (and make comparisons for) the path loss, K-factor and RMS delay spread. Our findings underscore the importance of accurately specifying the electrical properties of the surfaces (walls, etc.) in addition to their layouts.

There is related published work in this area. For urban microcell environments [8] shows very good agreement between the signal strength (or path loss) statistics of WiSE and those from extensive measurements. For indoor channels, [2] shows that the distributions of arrival times and angular spreads generated with WiSE agree very well with those of an empirical model based on measurements. In [9], extensive measurements in several office buildings are used to derive statistics for K factor and path loss, which favorably compare with WiSE predictions. All these results demonstrate the validity of using a ray tracing tool. In this paper, we add to prior results on K-factor and path loss; add new results for RMS delay spread; and show that a certain amount of preliminary trial-and-error (measurement, comparison and adjustment) can enhance the accuracy of such a tool.

Published models, whether stochastic or environment-specific, generally assume the channel response is non-varying over time if both ends of the path are fixed. However, in real environments channel response varies over time, e.g., due to movement of people in the environment. A question that has been open in the propagation community is whether this variation is negligible, and how it can be modeled in cases where the variation is not negligible. Here, we examine this problem as well. We have measured the channel response in an office building under different scenarios of environmental dynamics (i.e., movement of people), and we have identified stochastic processes to characterize them.

This paper combines and expands upon the results reported in [10] and [11], and is organized as follows: In Section II, we describe the measurement and ray-tracing simulation methods used here. Sections III and IV describe, respectively, K-factor estimations derived from channel response data and the estimation of RMS delay spread. Section V compares WISE predictions with VNA measurements in terms of path gain, K-factor and RMS delay spread. Section VI turns to time variations and defines four scenarios of motion in the wireless environment. Section VII explains the use of random processes to describe these time variations. Section VIII demonstrates our methodology for identifying the appropriate process for each motion scenario. Section IX summarizes our main findings.

II. Methodology

A. Measurements with a Vector Network Analyzer (VNA)

In our experiments, we measured the complex channel response with the vector network analyzer (VNA) Agilent E5071B. Measurements were carried out at various locations in the ORBIT room and office area of WINLAB, Rutgers University. The ORBIT room is of size 20 m$\times$25 m and it is surrounded by offices and hallways. The office area of WINLAB is as big as the ORBIT laboratory and contains cubicles, small rooms and lots of furniture.

All antennae were omnidirectional, at the same height, 1.25 m, and all transmit powers were 10 dBm. The VNA measured the complex frequency response at N equally spaced frequencies over a given frequency range. We did M trials at each specific location. The time duration between the contiguous trials was two seconds. This corresponds to the time spent for measuring the frequency response at N points, and then processing and transferring the data over the network. The impulse response in each trial was found via the inverse Fourier transform of the complex frequency response. The resulting time sequence, $h(n)$, represents the complex envelope of the response, sampled at 1-ns intervals and referred to 3.5 GHz. Each term in the sequence can be regarded as a ray.

B. Simulations with the WiSE Tool

We used WiSE [7] to simulate the static radio environment of the ORBIT room where we conducted the VNA measurements. Given a building plan and transmitter location, WiSE simulates the impulse response for any path in the building as a sum of rays. It accounts for the many rays that undergo reflection and transmission, where the number of reflections included per ray is a program input. It takes into account path loss and the wall layer properties, such as dielectric coefficient, width, conductivity, number of layers, etc. In WiSE, each wall is defined by its geometric layout and by a parameter called 'wall type'. An existing wall type can be redefined or a new wall type can be defined by declaring dielectric coefficients, width and conductivity for each layer of the wall.

III. K-factor Estimation Methods

A. Prior Work on Ricean K-factor Estimation

The K-factor is the ratio of the power in the line-of-sight (LOS) component to the total power of the non-LOS (NLOS) components. It is a measure of the extent of fading on the link, where lower K means deeper fading.

Various algorithms have been proposed to estimate the K-factor. The moment method reported in [12] estimates the K-factor from the second and fourth moments of the signal fading variation over time, space or frequency. It is more practical than many other proposed methods, as it requires power samples only (no phase). The moment method can be generalized to use with different moments, as in [13]. The authors in [13] also propose a K-factor estimation method using the in-phase and quadrature components, but this method is applicable only to narrowband signals. The method of maximum likelihood (ML) estimation of K-factor is proposed in [14], wherein the parameters of the Ricean distribution are chosen as those parameters which maximize the joint probability density of the observed outcomes.

B. Estimation from Impulse Responses

The channel impulse response gives the rays received at different delays. The ray that has the largest magnitude is designated as the line-of-sight "LOS" component. The power sum of the other remaining rays constitute the "scatter" power.

The ratio of the LOS ray's power to the scatter power gives the K-factor.

Note that the physical LOS component is almost always the one with the shortest delay. Thus, the power we use for the K-factor numerator may or may not be the actual LOS power. From the standpoint of estimating a K-factor that accurately predicts the fading distribution, however, this is an intuitive approach that (as we will show) leads to excellent results.

C. Estimation from Frequency Responses (Coherent Method)

The K-factor can be computed from the complex frequency response coherently. Assume we know the complex channel response $H(f)$ at M different frequencies. Let $V = |V|e^{-j\phi}$ be the complex amplitude of the LOS component. It can be estimated by minimizing the difference between the expected and measured channel response. Thus,

$$V^* = \arg\min_V E_f\{|H(f) - |V|e^{-j(2\pi f\tau+\phi)}|^2\} \quad (1)$$

where τ is the delay at which the LOS component is received. The solution V^* to this minimization problem is

$$V^* = E_f\{H(f)e^{j2\pi f\tau}\}, \quad (2)$$

where τ is found as

$$\tau^* = \arg\max_\tau E_f\{|H(f)e^{j2\pi f\tau}|\}. \quad (3)$$

This solution is equivalent to performing an inverse Fourier transform on the frequency domain data and choosing the largest component as the LOS component. Therefore, the coherent method gives the same result as estimating the numerator of the K-factor from the most powerful ray of the impulse response.

D. Estimation from Frequency Responses (Moment Method)

The moment method proposed in [12] assumed a temporal variation of the received signal. It uses the second and fourth moments of the magnitude variation over some long interval for the K-factor estimation. This method needs only the absolute values of the received signal samples. It is also applicable to frequency domain data, assuming a very wide bandwidth. Thus, the K-factor can be computed by computing second and fourth moments from the samples of $|H(f)|$.

This method loses precision at very low K-factors, i.e., $K \leq 1$. At the same time, the fading distribution does not change much over that range of K, so that imprecision in estimating K is not impactful.

IV. RMS Delay Spread

The RMS delay spread is a measure of the frequency selectivity (or pulse dispersion) of a link. Pulse dispersion arises as a result of the signals taking different times to cross the channel through different propagation paths. The RMS delay spread is defined as the second central moment of the power delay profile:

$$\tau_{rms} = \sqrt{\bar{\tau^2} - \bar{\tau}^2}, \quad (4)$$

where

$$\bar{\tau} = \frac{\sum_{n=1}^N P_n t_n}{\sum_{n=1}^N P_n}; \quad \bar{\tau^2} = \frac{\sum_{n=1}^N P_n t_n^2}{\sum_{n=1}^N P_n}; \quad (5)$$

N is the number of received rays; and P_n and t_n are, respectively, the power and arrival time of the n^{th} ray [1].

$$\tau_{rms} = \frac{1}{\sum_{n=1}^N P_n}\sqrt{\sum_{n=1}^N \sum_{m=n+1}^N P_n P_m (t_n - t_m)^2}. \quad (6)$$

We can rewrite (6) as

$$\tau_{rms} = \sqrt{\sum_{n=1}^N \sum_{m=n+1}^N \rho_n \rho_m (t_n - t_m)^2} \quad (7)$$

where ρ_x is the normalized power of x^{th} ray,

$$\rho_x = \frac{P_x}{\sum_{n=1}^N P_n}. \quad (8)$$

Clearly, $0 \leq \rho_x \leq 1$. From (7) it is obvious that RMS delay spread depends only on delay differences, and does not depend on where we set the origin, $\tau = 0$. It also does not depend on the transmit power, but solely on the power ratios of the rays.

V. Comparing VNA Data and WiSE Predictions

A. Transmitter-Receiver Paths Measured

We report here on VNA-WiSE comparisons for 18 different transmitter-receiver paths in the ORBIT lab. We repeated such experiments for various other paths and found similar results. Specifically, we measured the complex frequency response at 1601 points between 3.0 and 4.0 GHz. We repeated this VNA experiment 50 times for each path. Since the differences among the experiments were small, we show the results for only one of each path measurement. We chose the frequency range as 3-4 GHz to avoid interference from the widely used 2.4 and 5 GHz bands. Fig. 1 shows the 18 transmitter-receiver paths $T \rightarrow R$, $A \rightarrow B$ and from $T1 \rightarrow C$ to $T16 \rightarrow C$. T and R are 3.6 m apart; and A and B are 5.9 m apart. The transmitter locations $T1$ to $T16$ are located on a square of size 12.2 m x 12.2 m, where neighboring transmitter locations are about 3 m apart. The receiver location C is at the center of this square.

B. Wall Properties

The walls in the ORBIT lab are made of multiple layers of different materials used for isolation and shielding. Moreover, not every wall has the same layers; and we do not have exact information on the properties of these layers. Therefore, modeling of the walls is not straightforward. We considered, for each wall, various predefined wall types in WiSE. We have chosen those wall types for which preliminary experiments and comparisons between VNA and WiSE results showed the best agreement. For the ceiling and floor we chose a concrete wall

[1] We can regard P_n as the squared magnitude of the n^{th} ray in the impulse response, as described in Section II-A for the VNA data and in Section II-B for WISE. Also, N is not necessarily the same for the VNA-derived and WISE-derived impulse responses.

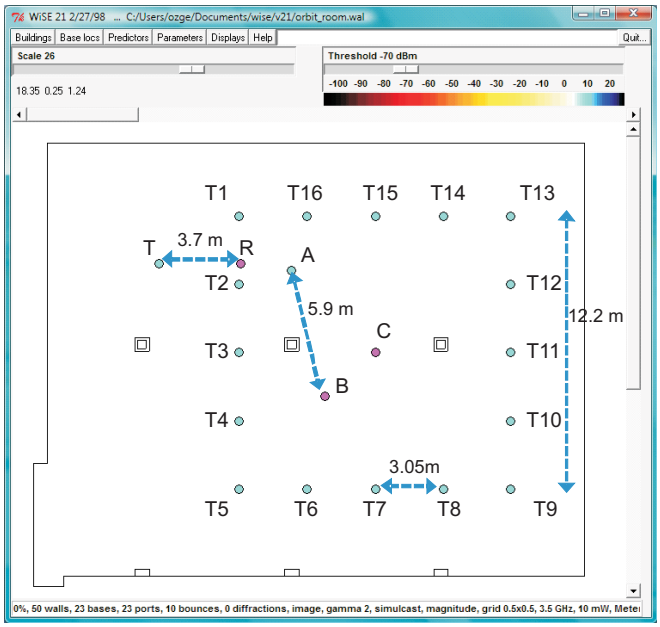

Fig. 1. Transmitter-receiver locations within ORBIT lab: $T \rightarrow R$, $A \rightarrow B$ and $T1 \rightarrow C$ to $T16 \rightarrow C$.

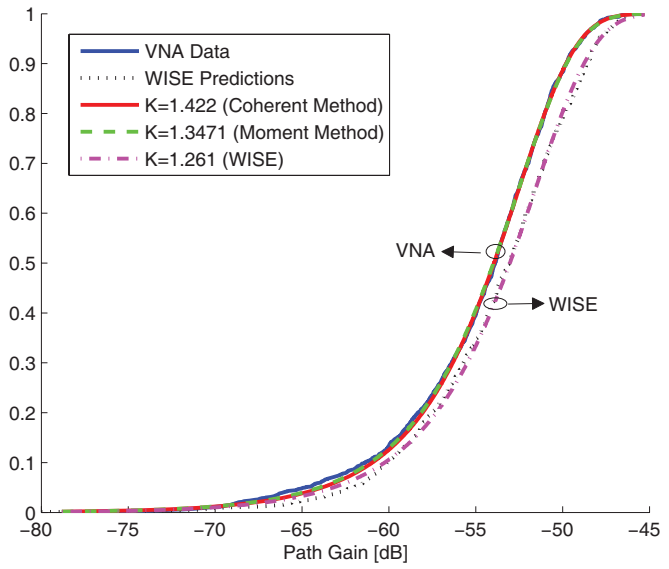

Fig. 2. Comparison of CDF's of path gain ($T \rightarrow R$). The curves shown with K-factor are the Ricean CDFs. The VNA-derived, and WISE-predicted CDFs look like one another and like the Ricean CDFs.

type; for the other walls, we chose metallic and sheetrock wall types.

The pillars on the radio path cause diffraction, reflection and transmission, which affect the received power significantly. Therefore, accurate modeling of the pillars is necessary. We modeled the pillar walls using a sheetrock wall type. We know that each pillar is built with a metallic block inside. Therefore, we added a second layer of walls made of metal inside the pillars. During our search for the best wall type combinations, we learned how critical the electrical properties of the walls are in addition to their geometric layout. We conclude that a certain amount of preliminary trial-and-error (measurement, comparison and adjustment) is needed for the prediction tool to be confidently applied.

C. Path Gain, K-factor and Fade CDFs

The cumulative distribution function (CDF) of the path gain (power ratio) can be obtained directly by sorting the measured or simulated frequency response samples. We call this the empirical CDF. A good fit to this curve is found in every case to be the theoretical Ricean CDF, parameterized only by the K-factor and average power gain.

Fig. 2 compares the path gain CDF's for the path $T \rightarrow R$. We see that the theoretical curves (obtained for K-factors estimated using either the moment method or the impulse response method) are very good matches to the empirical CDF's. Also, the WiSE-based and VNA-based CDF's of path gain are very close to each other. We obtained similarly good matches also for the other 17 links.

Table I summarizes the average path gains and the variation of the K-factors for the 18 paths considered. The measured and predicted values are seen to be in good agreement. Additionally, our results show that, in indoor environments, the K-factor is very low due to the transmissions through and reflections from the walls and objects in the surrounding. The maximum K-factor we saw was 1.42.

TABLE I
COMPARISION WISE AND VNA DATA

	Av. Path Gain [dB]		K		RMS d. s. [ns]	
	VNA	WiSE	VNA	WiSE	VNA	WiSE
T→R	-53.01	-52.04	1.42	1.26	41	34
A→B	-56.29	-55.18	0.58	0.82	58	48
T1→C	-56.07	-57.05	0.19	0.46	67	52
T2→C	-54.38	-56.52	0.20	0.82	62	51
T3→C	-56.86	-55.27	0.16	0.73	73	56
T4→C	-54.21	-55.97	0.28	0.66	60	53
T5→C	-55.55	-56.40	0.22	0.38	68	57
T6→C	-53.63	-55.44	0.24	0.54	61	61
T7→C	-53.18	-55.08	1.13	0.68	58	56
T8→C	-53.60	-55.76	0.30	0.61	60	56
T9→C	-54.21	-56.15	0.31	0.35	61	55
T10→C	-53.42	-55.51	0.53	0.56	65	58
T11→C	-56.96	-56.13	0.36	0.32	74	56
T12→C	-55.04	-55.99	0.30	0.67	71	57
T13→C	-57.74	-55.83	0.10	0.52	68	58
T14→C	-55.99	-55.69	0.13	0.59	66	52
T15→C	-55.13	-55.14	0.29	0.69	64	55
T16→C	-55.63	-55.23	0.08	0.50	64	54

D. RMS Delay Spread

The RMS delay spread, τ_{rms}, depends solely on the delay differences among the rays and on their relative powers, (7). Because the delay spread is based on moments of a function, impulse response rays at the larger delays can have an important impact on the calculated result, even if their powers are very low. The VNA-derived impulse response, being an inverse Fourier transform of measured frequency response samples, has rays out to a maximum delay dictated by the measurement bandwidth (1 GHz) and the number of samples (1601), i.e., out to 1.6 μs. This is much larger than the actual maximum delay in an indoor environment. The additional 'rays' in the VNA-derived impulse response are the result of measurement noise and other measurement artifacts.

To fairly compare the VNA-derived τ_{rms} with the value predicted using WiSE, we should use a maximum delay, t_η, that is common to both calculations. We chose the delay at which the WiSE ray powers drops permanently below -30 dB relative to the strongest ray in the impulse response. Thus, from both the VNA-derived and WiSE-predicted impulse responses, we calculate RMS delay spread using rays from relative delay 0 to relative delay t_η.

The RMS delay spreads for 18 links are shown in Table 1. They differ in most cases by 20 percent or less, with the VNA-derived estimates always being higher. In just a few cases, the VNA-derived value is as much as 30 percent higher.

The consistent increase of VNA-derived values over WiSE predictions may be due to imperfect calibration of the VNA data. The VNA-derived delay spread can be shown to be sensitive to calibration errors, and in a way that would increase its estimated value (c.f., [15]). Correcting for this impairment would improve the comparisons shown. This bears further study.

VI. Time Variations in Different Environments

A. Motivation and Goal

If there is considerable motion of people in an otherwise fixed wireless environment, there will be temporal changes in the response along a transmit-receive path, i.e., the static responses predicted using WiSE will not suffice to fully characterize the channel. We can envision the full response on a given path as being the sum of a static one (e.g., one predicted using site-specific ray tracing) plus a zero-mean time-varying one, based on some type of empirical model. More specifically, the time-varying part can be thought of as a set of time-varying processes added to the rays of the static part.

Some questions that arise are: Which rays (or taps of the effective impulse response) will be time-varying? What will be the relative strengths, e.g., the mean power of the time-varying part relative to the power of the static part? How will this ratio vary across taps? Can the time variations of the tap gains be modeled as random processes and, if so, what kind? How will the answers to these questions depend on the channel bandwidth, the specific site, the specific path, and the type of surrounding motion?

A full set of answers to these questions would lead to a highly useful model for the time-varying part of the wireless channel response. At the same time, acquiring these answers would take an extremely comprehensive measurement program spanning many environments, paths, motion scenarios and bandwidths. We have made numerous measurements, as we will report here, but not nearly enough to satisfy such requirements. Our less ambitious goal is to show, for some typical motion scenarios, that (1) only a few impulse response tap gains show significant variations; and (2) a well-known family of Gaussian random processes (the autoregressive processes, to be described later) can be used to characterize the time-varying nature of the tap gains. Since these findings apply across all the cases studied, we regard them as providing a highly useful starting point for time-variation modeling of indoor channels with fixed transmitter and receiver.

We defined four different kinds of motion scenarios-the static one (no motion) and three others-and we conducted a set of temporal measurements for each. The specific motion categories and the associated experiments are described next.

B. Measured Environments

Static Environment: We placed the antennae in the ORBIT room 3.65 m apart and measured the channel response at $N = 1601$ frequencies between 3.0 and 4.0 GHz. We repeated the measurement $M = 100$ times, at 2-second intervals. During the experiment, no one was present in the room.

Quasi-Static Environment: We placed the antennae in the ORBIT room 7.9 m apart and measured the channel response at $N = 1601$ frequencies between 3.0 and 3.1 GHz. We repeated the measurement $M = 600$ times, at 2-second intervals. During the experiment, 10-15 people were sitting around a table placed between the antennae and were eating lunch. Though they were sitting most of the time, people were also coming or leaving from time to time, as in a typical conference room scenario.

Random Movement: We placed the antennae in the ORBIT room 11.5 m apart and measured the channel response at $N = 401$ frequencies between 2.5 and 2.7 GHz. We repeated the measurement $M = 450$ times, at 2-second intervals. During the experiment, only one person was walking, running randomly between and around the antennae. There were no other people present in the room.

Office Space: This experiment was conducted in the office area of WINLAB. The receiver was placed near the door and the transmitter was placed at 10 m distance at a corner across. We measured the channel between 3.0 and 3.1 GHz at $N = 1601$ equidistant frequencies. We repeated the measurement $M = 750$ times, at 2-second intervals. During the experiment, 10-15 people were sitting in their cubicles and walking in and out from time to time.

These experiments were conducted at different times as part of different projects at our laboratory. For that reason, the combination of N, M and bandwidth, W, was different for each of the four above scenarios. The point we make here is that, despite differences in (N,M,W), the time variations of the tap gains for each category of people motion lend themselves to characterization by well-known random processes.

To study the four motion scenarios we defined and computed several quantities as follows: The total power gain (sum of squared magnitude of all impulse response components) is denoted by P_{trial} and is computed for each measurement (trial). The average of P_{trial} over the M measurements is denoted by P_{avr}. Departures of the set of P_{trial} values from P_{avr} reflect the temporal fluctuations of the ray (or tap) gains. The mean-square fluctuation of the n^{th} tap's squared magnitude about its average value is denoted by $\sigma_{tap}(n)$ or just σ_{tap}.

C. Results

1) Static Environment: In the static environment the channel response is nearly constant. P_{trial} deviates at most 1% from P_{avr}. The variations of the individual tap power gains are also negligible. σ_{tap} at the most variable tap corresponds

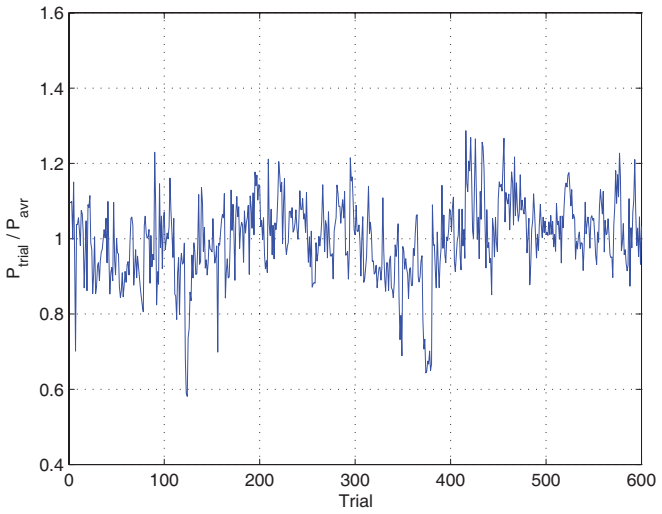

Fig. 3. Ratio of the trial power gain P_{trial} to the average power gain P_{avr} versus trials (quasi-static environment).

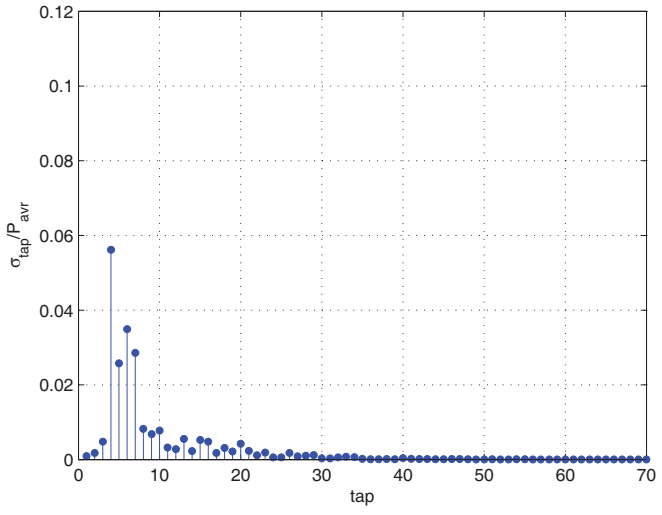

Fig. 4. Ratio of the tap power gain to average power gain versus tap number (quasi-static environment).

to only 0.3% of P_{avr}. Since the variations among the trials are insignificant, the channel response measured for one trial suffices to describe the environment. This was the case for the experiments that produce Table I.

2) Quasi Static Environment: Fig. 3 shows the ratio of P_{trial} to P_{avr} in the quasi-static environment. P_{trial} deviates up to 40% from P_{avr}. Fig. 4 shows σ_{tap} normalized by P_{avr}. Only four taps have σ_{tap}/P_{avr} greater than 2%. This 2% threshold is used here for comparing different environments, not for modeling purposes.

3) Random Movement: In this environment, P_{trial} deviates up to 20% from P_{avr}. The variation shows homogeneity, i.e., there are no trends or huge variations. Not all of the individual rays contribute to this variation in the same way. We plotted σ_{tap}, normalized by P_{avr} and saw that two taps contribute most to the variation of P_{avr}. For all other taps in this environment, σ_{tap} is less than 2% of P_{avr}.

The reasons that some of the tap gains show significant variation can be explained as follows. A moving object (e.g., a person or a clustered group of people) corresponds to one (or possible two) delay bins of the impulse response. The tap gain for each such delay bin will vary with time. For delays corresponding to non-moving objects, the tap gain will be essentially constant. The sets of time samples taken for the highly variable tap gains showed, in most cases, a reasonable conformity to a complex Gaussian distribution. This is likely due to the many returns from numerous scatterers (people), and the central limit theorem.

4) Office Space: In this environment, P_{trial} deviates up to 50% from P_{avr}. The variation has multiple means and slopes. We plotted the standard deviations of the tap power gains, σ_{tap}, normalized by P_{avr}, and saw that seven taps have normalized standard deviations greater than 2%.

VII. Time Variation Modeling

A. Prior Work on Autoregressive Processes

Autoregressive processes have been used for spectrum estimation purposes [16] and for modeling the variation of the channel response across frequencies [17]. In [17], the authors showed that a second-order AR process is sufficient to model the channel response across frequencies in a wideband indoor environment. Later, this approach was used in the ultra-wideband (UWB) channel modeling of indoor environments, [18]-[19]. A second-order AR process is proposed in [18] to capture the main characteristics of the UWB channel. In these studies, the frequency response is assumed to show insignificant change across time. To the best of our knowledge, autoregressive processes have not been used to characterize temporal variations of channel responses between fixed terminals.

B. Autoregressive Integrated Moving Average (ARIMA) Models of the Variations

We measure the complex channel response at N equally spaced frequency bins within a frequency range; we repeat this experiment M times within a time interval; and we define a matrix $\mathbf{H}$, where the entry in row i and column j corresponds to the complex channel response value at frequency f_i and trial t_j:

$$H(f_i, t_j) = \overline{H}(f_i) + \delta H(f_i, t_j) \quad i = 1 \ldots N \quad j = 1 \ldots M.$$

$\overline{H}(f_i)$ is the mean of a the channel response over M time instants at frequency f_i; $\delta H(f, t)$ is the time varying part; and we model $\delta H(f, t)$ through AR processes.

Specifically, we transform $\delta H(f, t)$ into the time domain and obtain $\delta h(n, t)$. The (complex) variation of $\delta h(n, t)$ at tap n across trials t constitutes a time series. We denote this time series as x, and we model it using ARIMA processes. We use the Box-Jenkins methodology, described in the Appendix, which also classifies the different members of the ARIMA family of processes.

VIII. ARIMA Modeling and Results

We now describe the modeling of x at a single tap in each environment. Models for the other significant taps can be

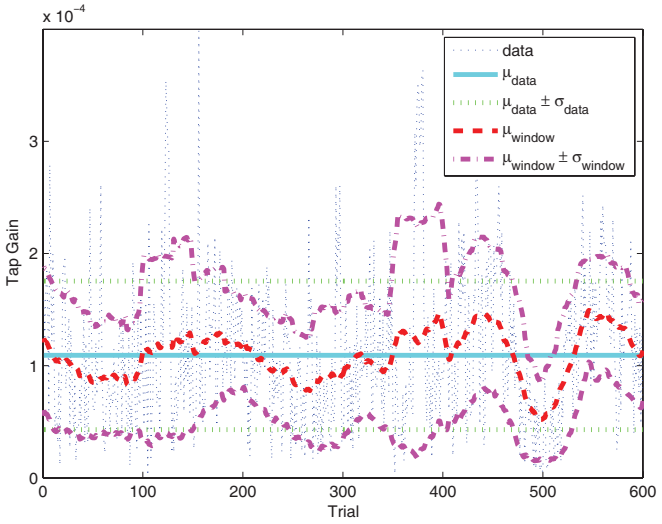

Fig. 5. Mean and standard deviation (quasi-static environment).

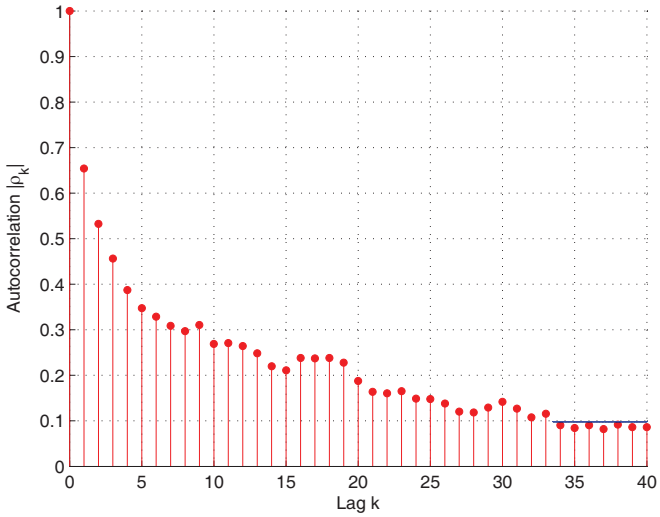

Fig. 6. Auto Correlation Function (quasi-static environment).

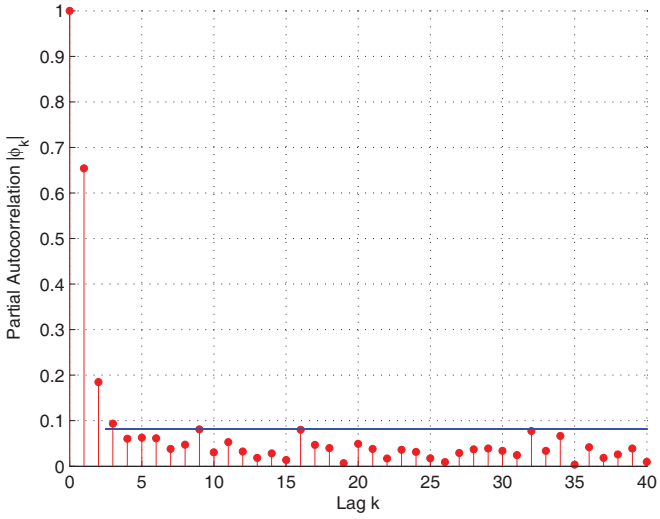

Fig. 7. Partial Correlation Function (quasi-static environment).

found in a similar way. We will demonstrate the Box-Jenkins methodology step by step as we find an appropriate model for the time variation in quasi-static environments. For the other environments, we will merely summarize the results.

A. *Quasi-Static Case*

Figure 4 shows that tap #4 is the most time-varying one in this case. We now model the discrete time series x for this tap.

1) Identification:

a) Mean and Variance: A stationary time series has the window mean and standard deviation agreeing with the overall data mean and variance to a great extent. We compute local means and variances of the absolute tap gain shown in Fig. 5 using sliding windows of size 50. 50% of the window mean samples deviate from the data mean by at most 15% and 90% of the window mean samples are within 30% of the data mean. Also, 90% of the window standard deviation samples are within 30% of the data standard deviation. This data can be classified as statistically stationary.

b) Auto Correlation Function (ACF): For an MA process of order q the ACF is zero after the lag q. For an AR process it decays to zero exponentially or as a mixture of damped sine waves. Figure 6 shows the ACF of x. The horizontal line at $|\rho_k| = 0.0982$ (starting at lag 34) shows the zero threshold computed using the Barlett approximation (Eq.(2.1.13) in [20]) which gives the variance of the estimated autocorrelation values ρ_k at lags beyond which the theoretical ACF may be deemed to have died out. The ACF decays exponentially and is effectively 0 after the lag 33.

c) Partial Correlation Function (PCF): For a stationary process X, the partial autocorrelation at the k^{th} lag is the correlation coefficient between X_1 and X_{k+1} after eliminating the effect of $X_2, \ldots, X_k$. For an AR process of order p, the PCF is zero after the lag p. Fig. 7 shows the PCF of x. The standard error σ of the estimated PCF values is approximately $1/\sqrt{n}$, where n is the number of samples. The horizontal 2σ lines are used as zero thresholds. The PCF is below the threshold after the third lag.

d) Choosing the possible models: Since the PCF is effectively zero after the third lag and the ACF tails off exponentially, we conclude that an AR(3) model is suitable. The value of PCF at the second lag is very small; therefore, the AR(2) model is also worth considering.

2) Estimating Parameters: We have estimated AR coefficients for the AR(2) and AR(3). The coefficients for the AR(2) model are $a_2(1) = 1.0000$, $a_2(2) = -0.5346 + 0.0249i$, $a_2(3) = -0.1833 - 0.0235i$. The coefficients for the AR(3) model are $a_3(1) = 1.0000$, $a_3(2) = -0.5175 + 0.0221i$, $a_3(3) = -0.1332 - 0.0228i$, $a_3(4) = -0.0934 + 0.0032i$.

3) Diagnostic Check: The AR(2) model and the AR(3) model in Fig. 8 show variations similar to those of the data. Choosing either one of them would not make much difference. For the cases where it is not so obvious which model is better, it is useful to have a criterion which indicates the appropriate model. We used the Akaike Information Criterion (AIC) to compare the models [21]. The AIC was derived by minimizing an information theoretic function, and it includes a penalty term for extra AR coefficients. The model which has

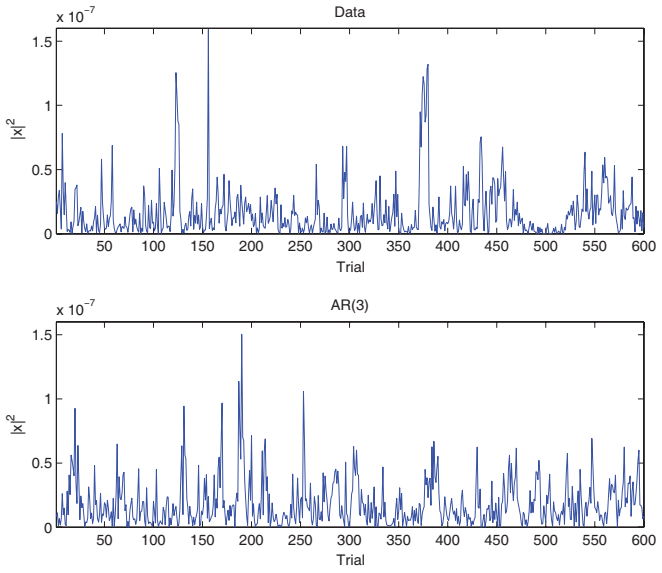

Fig. 8. AR(3) process compared with data (quasi-static environment).

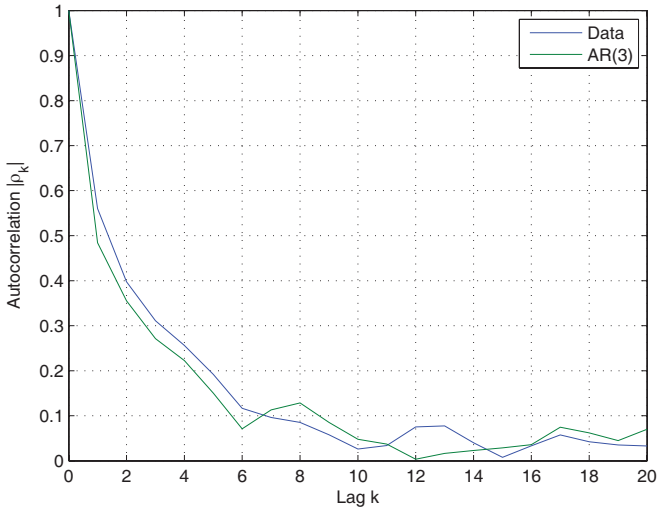

Fig. 9. Comparison of autocorrelation function of the data and AR(3) process (quasi-static environment).

the lowest AIC metric is chosen. In this case, the AIC was nearly the same for both models: For the AR(2) model, it was -15.68, and for the AR(3) model, it was -15.69.

The comparison of autocorrelation functions the data x and of the AR(3) process is shown in Fig. 9. The autocorrelation function of the AR process has a similar decay as the data.

B. Random-Movement Case

Here, we modeled x at the third most varying tap. For this tap, 90% of the window mean samples deviate from the data mean by at most 18%; and 90% of the window standard deviations are within 17% of the data standard deviation. Thus, the window mean and standard deviation agree to a great extent with the data mean and standard deviation, so the process is deemed to be stationary. The ACF in this case tails off as a mixture of exponential decays and damped sine waves.

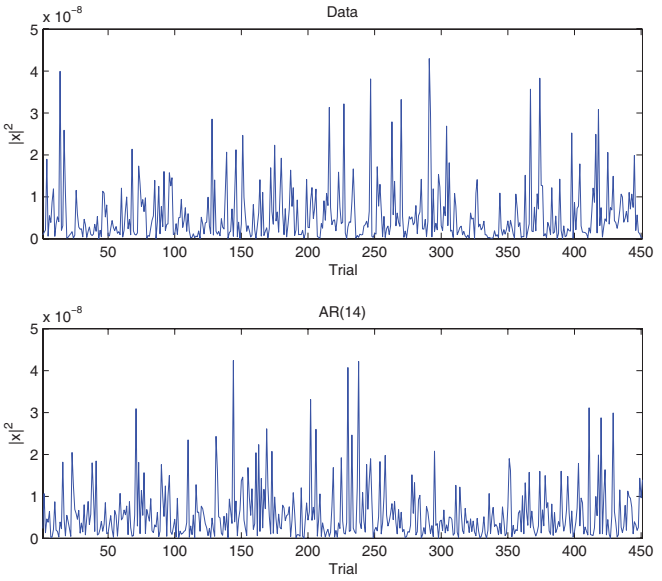

Fig. 10. AR(14) process compared with data (random movement).

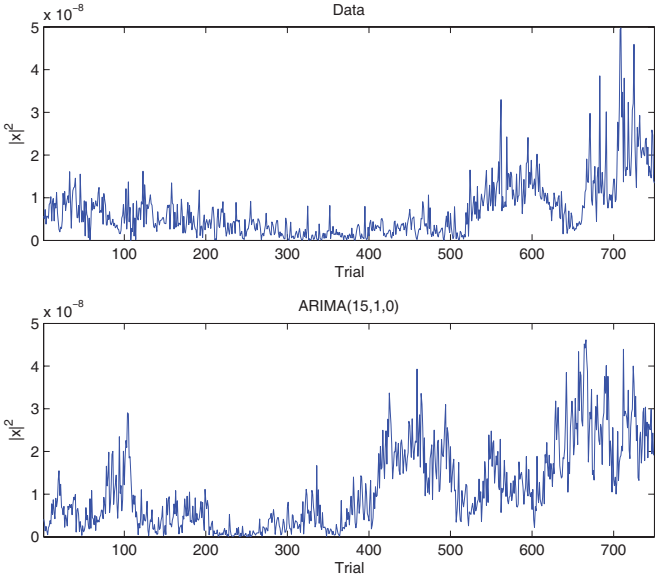

Fig. 11. ARIMA(15,1,0) model compared with data (office space).

The PCF is zero after the first tap. Fig. 10 shows an AR(14) process which has variations similar to measured data.

C. Office Space

Here, we modeled x at the most varying tap. The mean function in this case is not constant. Moreover, the all-pole model has poles outside the unit circle. Therefore, the process is not stationary. We applied a difference operator and investigated stationarity again.

To begin, we compared the window means and standard deviations with those for the first order difference ∇x. The local standard deviations were found to be close to those for the data. The all-pole model now has all of the poles inside the unit circle. The window mean is close to zero, which is also the data mean. Therefore, the first order difference process ∇x is deemed to be stationary.

Next, we find an ARMA model for ∇x. The ACF of ∇x initially decays exponentially and then tails off as damped sine waves. The PCF has an exponential-dominated decay. It is effectively zero after lag 11. We choose an ARIMA(15,1,0) process here, as shown in Fig. 11.

IX. Conclusion

The comparisons in Table I for the 18 paths we studied show that, the parameters predicted using WiSE agree well with measurements. This suggests that a well-designed ray-tracing program such as WiSE can be used with confidence for studying systems in indoor wireless environments.

In the course of our investigation, we identified two conditions that can compromise prediction accuracy of critical path properties: (1) Paths where diffraction is the primary propagation mechanism; and (2) environments for which the material properties of the walls, floor and ceiling are not well-specified. The first condition is relatively rare in indoor environments; the second condition can be avoided by using a small number of preliminary measurements, augmented by comparisons with predictions and corresponding adjustments of the assumed material properties.

Further work in this area should include, primarily, its extension to other paths and to other indoor environments. In addition, a limited amount of system studies would help to test the conjecture that the parameters studied here (path gain, K-factor and RMS delay spread) comprise a sufficient set for capturing the properties of a channel response.

We have shown that the time variations of the channel response in an indoor environment are not negligible in common scenarios such as people sitting around a table or working in an office. We stochastically modeled the time variation of the channel response about the mean using members of the ARIMA family of processes and showed that this can lead to an accurate representation. Our key finding is that ARIMA processes are capable of describing the time variation of the impulse response terms in these environments. We obtained excellent agreement using such processes for each of the categories identified and measured. Thus, one can choose to model the static indoor channel response through environment simulators and the fluctuation about it through ARIMA processes.

Acknowledgements

We are grateful to Dmitry Chizhik, Jonathan Ling and Reinaldo Valenzuela, all of Alcatel-Lucent, for many fruitful discussions on the uses of the WiSE tool.

Appendix

A. The Autoregressive (All-Poles) Processes, AR

The AR model pertains to an all-pole transfer function. A wide sense stationary AR process of order p is generated by passing a white noise sequence through an all-pole filter with a transfer function

$$H(z) = \frac{1}{1 + \sum_{k=1}^{p} a_p(k) z^{-k}}, \tag{A-1}$$

where $a_p(k)$ is the k^{th} AR coefficient of the p^{th}-order filter.

The Yule Walker equations [16] provide a relationship between the filter coefficients and the autocorrelation sequence. The AR coefficients are determined by solving these equations.

B. The Moving Average (All-Zeroes) Processes, MA

The MA process refers to an all-zero transfer function. This process is generated by passing a white noise sequence through a finite impulse response (FIR) filter having a transfer function

$$H(z) = 1 + \sum_{k=1}^{q} b_q(k) z^{-k}. \tag{A-2}$$

The Yule Walker equations for MA process are nonlinear in the model coefficients, b_q. To avoid solving non-linear equations, the coefficients can be determined from the coefficients of a higher-order all-pole filter[16].

C. The Autoregressive Moving Average Proceses, ARMA

The ARMA process refers to the general case of a transfer function with both poles and zeros. A wide sense stationary ARMA (p,q) autoregressive process can be generated by passing a white noise sequence through a filter having p poles and q zeros:

$$H(z) = \frac{1 + \sum_{k=1}^{q} b_q(k) z^{-k}}{1 + \sum_{k=1}^{p} a_p(k) z^{-k}} \tag{A-3}$$

An AR process is a special case of ARMA with $q = 0$; and an MA process is a special case of ARMA with $p = 0$. The filter coefficients a_q and b_q can be estimated solving Modified Yule Walker Equations (MYWE) [16].

D. ARIMA

A desired property in applying a time series model is statistical stationarity. Usually stationary time series can be described by their fixed mean, fixed variance and autocorrelation function. Many empirical series do not have a fixed mean even though they exhibit homogeneity apart from local level or trend. To make these time series stationary, the difference operator ∇ is applied d times until the data become stationary. The difference operator is defined as $\nabla x(n) = x(n) - x(n-1)$. Assume that, for a series of the d^{th} order difference, a stationary ARMA(p,q) model is obtained. The model for the nonstationary series can then be found by integrating this ARMA(p,q) process d times. Such processes are called Autoregressive Integrated Moving Average (ARIMA) (p,d,q). It is easy to see that ARIMA is the most general class, with ARMA being the subset of ARIMA for which $d = 0$.

The entire family of models called ARIMA was proposed by Box and Jenkins [20] and is applicable to a wide variety of situations. The Box-Jenkins technique is a methodology for constructing an ARIMA process to characterize a given time series. It involves a three-step procedure, consisting of identification, model estimation and diagnostics. Identification techniques are used to find out what particular kind of process is appropriate. They make use of the autocorrelation and partial autocorrelation functions. In the model estimation step, the parameters for each process are estimated. To find out if the fitted process adequately represent the data, diagnostic checks are done. If the fit is not good, the steps are repeated again.

E. The Autoregressive (All-Poles) Processes, AR

The AR model pertains to an all-pole transfer function. A wide sense stationary AR process of order p is generated by passing a white noise sequence through an all-pole filter with a transfer function

$$H(z) = \frac{1}{1 + \sum_{k=1}^{p} a_p(k) z^{-k}}, \tag{A-1}$$

where $a_p(k)$ is the k^{th} AR coefficient of the p^{th}-order filter.

The Yule Walker equations [16] provide a relationship between the filter coefficients and the autocorrelation sequence. The AR coefficients are determined by solving these equations.

F. The Moving Average (All-Zeroes) Processes, MA

The MA process refers to an all-zero transfer function. This process is generated by passing a white noise sequence through a finite impulse response (FIR) filter having a transfer function

$$H(z) = 1 + \sum_{k=1}^{q} b_q(k) z^{-k}. \tag{A-2}$$

The Yule Walker equations for MA process are nonlinear in the model coefficients, b_q. To avoid solving non-linear equations, the coefficients can be determined from the coefficients of a higher-order all-pole filter[16].

G. The Autoregressive Moving Average Proceses, ARMA

The ARMA process refers to the general case of a transfer function with both poles and zeros. A wide sense stationary ARMA (p,q) autoregressive process can be generated by passing a white noise sequence through a filter having p poles and q zeros:

$$H(z) = \frac{1 + \sum_{k=1}^{q} b_q(k) z^{-k}}{1 + \sum_{k=1}^{p} a_p(k) z^{-k}} \tag{A-3}$$

An AR process is a special case of ARMA with $q = 0$; and an MA process is a special case of ARMA with $p = 0$. The filter coefficients a_q and b_q can be estimated solving Modified Yule Walker Equations (MYWE) [16].

H. ARIMA

A desired property in applying a time series model is statistical stationarity. Usually stationary time series can be described by their fixed mean, fixed variance and autocorrelation function. Many empirical series do not have a fixed mean even though they exhibit homogeneity apart from local level or trend. To make these time series stationary, the difference operator ∇ is applied d times until the data become stationary. The difference operator is defined as $\nabla x(n) = x(n) - x(n-1)$. Assume that, for a series of the d^{th} order difference, a stationary ARMA(p,q) model is obtained. The model for the nonstationary series can then be found by integrating this ARMA(p,q) process d times. Such processes are called Autoregressive Integrated Moving Average (ARIMA) (p,d,q). It is easy to see that ARIMA is the most general class, with ARMA being the subset of ARIMA for which $d = 0$.

The entire family of models called ARIMA was proposed by Box and Jenkins [20] and is applicable to a wide variety of situations. The Box-Jenkins technique is a methodology for constructing an ARIMA process to characterize a given time series. It involves a three-step procedure, consisting of identification, model estimation and diagnostics. Identification techniques are used to find out what particular kind of process is appropriate. They make use of the autocorrelation and partial autocorrelation functions. In the model estimation step, the parameters for each process are estimated. To find out if the fitted process adequately represent the data, diagnostic checks are done. If the fit is not good, the steps are repeated again.

REFERENCES

[1] M. Hassan-Ali and K. Pahlavan, "A new statistical model for site-specific indoor radio propagation prediction based on geometric optics and geometric probability," *IEEE Trans. Wireless Commun.*, vol. 1, pp. 112–124, 2002.

[2] G. German, Q. Spencer, L. Swindlehurst, and R. Valenzuela, "Wireless indoor channel modeling: statistical agreement of ray tracing simulations and channel sounding measurements," in *Proc. IEEE International Conference on Acoustics, Speech, and Signal Processing*, 2001, pp. 2501–2504.

[3] M. Hassan-Ali and K. Pahlavan, "Site-specific wideband and narrowband modeling of indoor radio channel using ray-tracing," in *Proc. Ninth IEEE International Symposium on Personal, Indoor and Mobile Radio Communications 1998*, vol. 1, pp. 65–68, Sept. 1998.

[4] E. C. K. Lai, M. J. Neve, and A. G. Williamson, "Identification of dominant propagation mechanisms around corners in a single-floor office building," in *Proc. Antennas and Propagation Society International Symposium*, pp. 1–4, July 2008.

[5] J. Lei, R. Yates, L. Greenstein, and H. Liu, "Mapping link SNRs of wireless mesh networks onto an indoor testbed," *Conf. Rec. of TridentCom*, Mar. 2006.

[6] M. Ott, I. Seskar, R. Siracusa, and M. Singh, "ORBIT Testbed Software Architecture: Supporting experiments as a service," in *Proc. IEEE Tridentcom*, Feb. 2005.

[7] S. Fortune, D. Gay, B. Kernighan, O. Landronand, R. Valenzuela, and M. Wright, "WISE design of indoor wireless systems: practical computation and optimization," *IEEE Computational Science and Engineering*, vol. 2, no. 1, pp. 58–68, 1995.

[8] V. Erceg, S. Fortune, J. Ling, J. Rustako, A. J., and R. Valenzuela, "Comparisons of a computer-based propagation prediction tool with experimental data collected in urban microcellular environments," *IEEE J. Select. Areas Commun.*, vol. 15, no. 4, pp. 677–684, May 1997.

[9] R. Valenzuela, D. Chizhik, and J. Ling, "Measured and predicted correlation between local average power and small scale fading in indoor wireless communication channels," in *Proc. IEEE 48th Vehicular Technology Conference*, vol. 3, pp. 2104–2108, May 1998.

[10] A. O. Kaya, L. Greenstein, and W. Trappe, "Characterizing indoor wireless channels via ray tracing, and validation via measurements," *GLOBECOM'08*, Nov. 2008.

[11] ——, "Modeling temporal channel variations in indoor wireless environments," *MILCOM'08*, Nov. 2008.

[12] L. Greenstein, D. Michelson, and V. Erceg, "Moment method estimation of the Ricean K-factor," *IEEE Commun. Lett.*, vol. 3, pp. 175–176, June 1999.

[13] C. Tepedelenlioglu, A. Abdi, and G. Giannakis, "The Ricean K factor: estimation and performance analysis," *IEEE Trans. Commun.*, vol. 2, pp. 799–809, July 2003.

[14] K. Talukdar and W. Lawing, "Estimation of the parameters of the Rice distribution," *J. Acoust. Soc. Am.*, vol. 89, no. 3, pp. 1193–1197, Mar. 1991.

[15] A. Saleh and R. Valenzuela, "A statistical model for indoor multipath propagation," *IEEE J. Select. Areas Commun.*, vol. 5, no. 2, pp. 128–137, Feb. 1987.

[16] M. H. Hayes, *Statistical Digital Signal Processing and Modeling*. New York: John Wiley Sons, 1996.

[17] S. Howard and K. Pahlavan, "Autoregressive modeling of wide-band indoor radio propagation," *IEEE Trans. Commun.*, vol. 40, no. 9, pp. 1540–1552, Oct. 1992.

[18] S. Ghassemzadeh, J. R., C. Rice, W. Turin, and V. Tarokh, "Measurement and modeling of an ultra-wide bandwidth indoor channel," *IEEE Trans. Commun.*, vol. 52, no. 10, pp. 1786–1796, Oct. 2004.

[19] Z. Irahhauten, H. Nikookar, and G. J. M., "An overview of ultra wide band indoor channel measurements and modeling," *IEEE Microwave and Wireless Components Lett.*, vol. 14, no. 10, pp. 386–388, Aug. 2004.
[20] G. E. P. Box and G. M. Jenkins, *Time Series Analysis Forecasting and Control*. San Francisco CA: Holden-Day Inc., 1976.
[21] H. Akaike, "A new look at the statistical model identification," *IEEE Trans. Automatic Control*, vol. AC-19, pp. 716–723, 1974.

Aliye Özge Kaya received her BSc. and Dipl.-Ing. in Electrical and Information Technology Engineering from the Munich University of Technology (TUM), Munich, Germany, in 2003. She is currently working towards her Ph.D. at the Wireless Information Networks Laboratory (WINLAB), Rutgers University, NJ. In 2006 she was a summer intern at InterDigital Inc., PA working in design and implementation of 3GPP GERAN systems. She worked on wireless localization in 2005 at Alcatel-Lucent Bell Labs, NJ. Her research interests include radio channel modeling, MIMO-based systems, wireless localization and P2P-ISP networks.

Larry J. Greenstein received the B.S., M.S., and PhD degrees in electrical engineering from Illinois Institute of Technology, Chicago, IL, in 1958, 1961, and 1967, respectively. From 1958 to 1970, he was with IIT Research Institute, Chicago, IL, where he conducted research on radio frequency interference and anti-clutter airborne radar. He joined Bell Laboratories, in Holmdel, NJ, in 1970. Over a 32-year AT&T career, he conducted research on digital satellites, point-to-point digital radio, optical transmission techniques, and wireless communications. For 21 years during that period (1979-2000), he led a research department renowned for its contributions in these fields. He is now a Research Professor at Rutgers-WINLAB, North Brunswick, NJ, working in the areas of cognitive radio, sensor networks, MIMO-based systems, Broadband Power Line systems and radio channel modeling.

Dr. Greenstein is an AT&T Fellow, recipient of the IEEE Communications Society's Edwin Howard Armstrong Award, and winner of four best paper awards. He is currently Director of Journals for the IEEE Communications Society and has been a Guest Editor, Senior Editor and Editorial Board Member for numerous publications.

Wade Trappe received his B.A. degree in Mathematics from The University of Texas at Austin in 1994, and the Ph.D. in Applied Mathematics and Scientific Computing from the University of Maryland in 2002. He is currently an associate professor in the Electrical and Computer Engineering Department at Rutgers University, and is Associate Director of the Wireless Information Network Laboratory (WINLAB). His research interests include wireless security, wireless networking, multimedia security, and network security. While at the University of Maryland, Dr. Trappe received the George Harhalakis Outstanding Systems Engineering Graduate Student award. Dr. Trappe is a co-author of the textbook Introduction to Cryptography with Coding Theory, Prentice Hall, 2001. He is the recipient of the 2005 Best Paper Award from the IEEE Signal Processing Society. He is a member of the IEEE Signal Processing and Communications societies, and a member of the ACM.